Nanoscale mapping of photo-induced charge carriers generated at interfaces of a donor/acceptor 2D-assembly by light-assisted- scanning tunneling microscopy

Andrés Lombana, Nicolas Battaglini, Samia Zrig, Jérôme Lagoute, Alexandre Chevillot-Biraud, Philippe Lang

Nanoscale mapping of photo-induced charge carriers generated at interfaces of a donor/acceptor 2D-assembly by light-assisted-scanning tunneling microscopy

Andrés Lombana Nicolas Battaglini Samia Zrig Jérôme Lagoute Alexandre Chevillot-Biraud Philippe Lang**

Dr. A. Lombana, Dr. N. Battaglini, Dr. S. Zrig, Dr. J. Lagoute, A. Chevillot-Biraud, Dr. P. Lang
Université de Paris, ITODYS, CNRS, F-75006 Paris, France
Email Address: nicolas.battaglini@u-paris.fr; lang@univ-paris-diderot.fr
Dr. J. Lagoute
Université de Paris, MPQ, CNRS, F-75006 Paris, France

Keywords: *supramolecular assembly, donor/acceptor system, light-assisted scanning tunneling microscopy, photocurrent, charge transfer, molecular and organic electronics*

We have investigated charge transfers between donor (D) and acceptor (A) species at their excited state in a light-assisted STM setup (LA-STM). Through an all-solution process, we have elaborated supramolecular architectures deposited on the Au(111) surface and made of 2D islands of $PC_{71}BM$ (electron acceptor) on top of a single layer of the polymer PTB7 (electron donor). The STM junction under modulated laser irradiation exhibits a strong background of photothermal signal attributed both to vertical and lateral expansion of the tip. However, from the analysis of differential images obtained at opposite voltages, we have been able to detect additional photocurrent peaks located at the PTB7/$PC_{71}BM$ interfaces, providing evidence for active charge transfer between D/A species at their excited state. We discuss this phenomenon in the framework of a charge transport model at interfaces in organic electronics systems.

1 Introduction

The comprehensive understanding of light/matter interactions plays a central role in areas such as organic and hybrid photovoltaics. The properties and performance of photoactive systems often rely on processes that operate at the nanoscale.[1] However, the direct mapping of localized photo-induced charge transfer between molecular species still remains a major challenge. At the nanometric scale, the observation and understanding of such phenomenon requires the use of local-probe-based techniques.[2] Several experimental approaches have been developed to extract an electrical or optical signal specifically related to absorption and excitation phenomena in photo-active molecular systems. On the one hand, the observation of the electroluminescent phenomenon under the tip of a scanning tunneling microscope (STM) has been successfully applied to the measurement of energy transfers between adsorbed molecules with a submolecular resolution.[3] This technique consists in analyzing the photons emitted during an inelastic tunnel transition through the electronic levels of the probed molecules. Moreover, it has been shown that the tip/surface gap can be used as a plasmonic cavity to generate the electroluminescence of the organic layer.[4] On the other hand, the detection of photo-induced surface charges by electrostatic force microscopy (EFM) or Kelvin Probe microscopy (KPFM) has been employed to study the charge generation in the active organic film of a bulk heterojunction photovoltaic cell.[5, 6, 7] In such phase-separated donor/acceptor composites, KPFM under illumination measures the variation of the surface photo-voltage (SPV) due to the presence of opposite charge carriers respectively in the LUMO of the acceptor and in the HOMO of the donor.[8] A third method is to detect the current resulting from the photoexcitation of the organic material in the STM junction under light irradiation. Among the various photo-induced phenomena that can be observed with this technique,[9, 10] the light assisted STM (LA-STM) configuration was notably used to detect the heat dissipation caused by the absorption of the electromagnetic energy absorbed by the irradiated molecules, both in the visible range,[11] and in the infra red domain.[12] LA-STM has also been used to map the photocurrent resulting from the resonant optical excitation of adsorbed semiconducting molecules,[13] or to detect the photogeneration of charge carriers and to locate exciton recombination regions on the surface of an organic semiconducting thin film.[14]

The group of W. Ho has shown that the absorption of a photon by a molecule involves a tunnel transport mechanism through its excited levels.[15] LA-STM has also been extended to the characterization of light absorption by individual inorganic nanostructures such as carbon nanotubes,[16] and quantum dots.[17]
In this framework, we have developed a LA-STM setup that aims at mapping the photocurrent resulting from charge transfer at the local scale between a monolayer of a donor polymer: the poly(4,8-bis[(2-ethylhexyl)oxy]benzo[1,2-b:4,5-b']dithiophene-2,6-diyl-alt-3-fluoro-2-[(2-ethylhexyl)carbonyl] thieno[3,4-b]thiophene-4,6-diyl), called PTB7, and an acceptor species: the [6,6]-phenyl-C_{71}-butyric acid methyl ester, called $PC_{71}BM$, both successively deposited on the Au(111) surface. Bulk-heterojunctions-OPV-cells based on the PTB7/PCBM couple are known for achieving high power conversion efficiencies.[18] As the interfacial area of the donor/acceptor domains has been pointed out as one of the key factors to improve the efficiency of organic photovoltaic devices,[19, 20, 21, 22, 23, 24] we have first carried out a systematic analysis of the morphology of the bi-component film, that we obtained from a solution deposition approach. Then, we have compared the behavior of the PTB7/$PC_{71}BM$ system under light irradiation with that of a non-photo-active self-assembled monolayer (SAM) of adamantanethiol (AT). Doing so, we have been able to highlight a combination of photo-induced effects from which we have extracted, in the case of the D/A system only, a signal located at D/A interfaces and consistent with charge transfers in the excited state between PTB7 and $PC_{71}BM$. Our model of the molecular system in the STM junction under light irradiation demonstrates that such photocurrent could originate from a perturbation of the electronic transport through partially occupied LUMO levels of the molecules.

2 Results and discussion

2.1 Supramolecular assemblies of the donnor/acceptor systems on Au(111)

2.1.1 PTB7 monolayer

The STM image of **Figure 1 (a)** shows the overall organization of PTB7 on Au(111). The molecular structure of the PTB7 monomer is sketched in **Figure 1 (c)**.
Polymer chains appear as bright strands separated by dark ones. For local density of states reasons, we attribute the bright lines to the aromatic part of the molecule whereas the dark ones correspond to regions where the aliphatic side chains interact and interdigitate. PTB7 locally forms 2D crystals comprising 3 to 4 strands of polymer in trans conformation, observable as zigzag lines. Here, the bright-to-bright distance is 1.77 ± 0.08 nm (**Figure 1 (b)**). The spatial extension of these crystallized areas does not exceed 10 nm. This value is in good agreement with the simulated persistence length of the polymer in the glass phase.[25] The orientation of the domains relative to each other is a multiple of 30°, as observed for P3HT on Au (111) or HOPG.[26, 27] This behavior is the fingerprint of the interaction of the polymer with the surface symmetry. Unlike P3HT, one also observe some hairpin curves (noted by the black ovals in **Figure 1 (a)**). In this type of folding, the diameter of curvature is greater than the interchain distance measured in the crystallized areas, leading to a local lowering of the polymer density. To achieve such hairpin bends, the polymer chain should adopt the *cis* conformation between neighboring monomers. A large diameter of curvature demonstrates the stiffness of the monomer. For comparison, W. Chen et al. have shown by X-ray scattering measurements that in the active layer of a photovoltaic cell,[28] PTB7 interchain distances lie in between 1.71 and 1.98 nm, depending on the solvent used to elaborate the bulk heterojunction layer. In the former case, side chains interdigitation is strong, whereas in the latter, it is weak. Our results on the 2D system at the interface with gold are in good agreement, with relatively strong side chain interactions. W. Chen et al. have also evaluated the size of the 3D crystals. They found approximately 3 to 4 nm, which corresponds to 2 or 3 juxtaposed chains. This tends to show that the behavior of PTB7 on Au(111) is close to the one observed in the bulk phase. It should be noted that PTB7 spontaneously forms crystallites of the order of magnitude of the diffusion length of an exciton, *i.e.* between 1 and 10 nm.

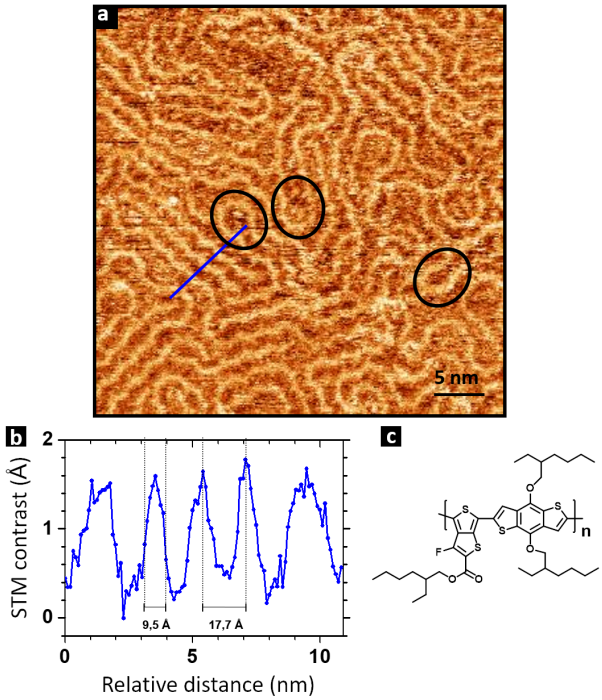

Figure 1: (a) STM image (40×40 nm^2, $V_t = 0.3$ V; $I_t = 50$ pA) showing the contrast of PTB7 chains on Au(111). Black ovals point out hairpin curves followed by the polymer chain. The blue line, perpendicular to a periodic PTB7 domain, indicates the position of the cross section presented in (b). (c) Chemical structure of the PTB7 monomer.

2.1.2 $PC_{71}BM$ monolayers

The self-organization of drop cast $PC_{71}BM$ on Au(111) leads to compact crystalline domains exhibiting an hexagonal network surrounded by amorphous or "glassy" areas. The spatial extension of ordered domains is larger than 20 nm. **Figure 2 (a)** and **(b)** show the molecular arrangement of $PC_{71}BM$ (sketched in **Figure 2 (c)**) inside an ordered island. The nearest neighbors distance is $a = 1.05 \pm 0.08$ nm. In **Figure 2 (a)**, one can also notice random contrast fluctuations between $PC_{71}BM$ entities.

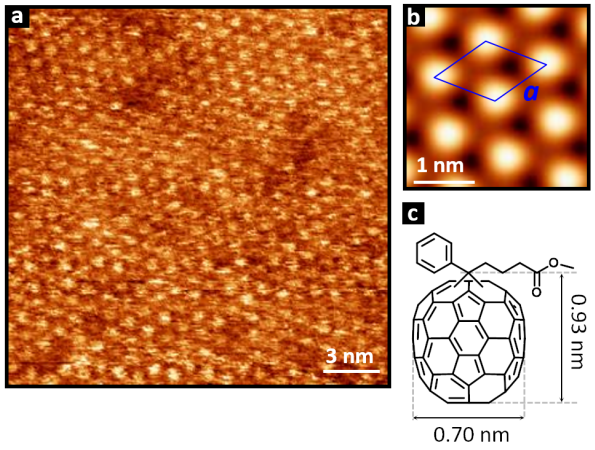

Figure 2: (a) STM images (20×20 nm^2; $V_t = 0.3$ V; $I_t = 8$ pA) showing the crystal structure of the $PC_{71}BM$ monolayer on Au(111). (b) Filtered magnified image showing the hexagonal packing (of lattice parameter a) adopted by $PC_{71}BM$ entities. (c) Chemical structure of $PC_{71}BM$[29].

The self-assembly of this molecule on Au(111) is poorly reported in the literature. However, the growth of fullerene derivatives and especially $PC_{61}BM$ on Au(111) has been addressed by UHV STM and relies mainly on the surface coverage.[30] For less than 0.5 monolayer, the self-ordering is driven by molecule-

substrate interactions influenced by the herringbone pattern of the reconstructed Au(111) surface. The organic tail of $PC_{61}BM$ plays a crucial role in the formation of double rows of molecules.[31] For higher coverages, $PC_{61}BM$ spontaneously forms organized domains exhibiting an hexagonal symmetry, separated by glassy areas.[32, 33] The phase transition occurs when the molecule-molecule interactions become predominant due to the increase of $PC_{61}BM$ density. All in all, our results for drop cast $PC_{71}BM$ monolayers follow the same trend. Nevertheless, no STM contrast fluctuation has been reported for spherical $PC_{61}BM$. For our system, this is probably the consequence of diverse adsorption geometries due to the ellipsoidal shape of the C_{70} fullerene.

2.1.3 PTB7/$PC_{71}BM$ systems

The drop casting of $PC_{71}BM$ above the PTB7 layer on Au(111) leads to the formation of a D/A system. The concentration gradient that occurs upon drying leads to local variations of the molecular density. The STM image of **Figure 3 (a)** highlights the main topographic features of the D/A system obtained at a $PC_{71}BM$ coverage ratio of *ca.* 30%. 2D Areas of $PC_{71}BM$ up to 10 nm in diameter appear as bright protrusions on a dark background where the PTB7 chains can be clearly distinguished. Here, $PC_{71}BM$ preferentially forms bundles of 2 to 10 units.
The topographic profile of **Figure 3 (a)** shows that the distance between adjacent $PC_{71}BM$ molecules is approximately 1.8 nm, which is larger than the separation found for the same layer on bare Au(111). However, this is very close to PTB7 interchain distance, demonstrating the ability of PTB7 to act as a template for the growth of $PC_{71}BM$ islands. In the literature, fullerenes deposited on polymers, especially polythiophene derivatives, also exhibit the same behavior, either for linear chains or macrocyclic oligomers.[34, 35] The magnified image of **Figure 3 (c)** shows that preferential adsorption sites for $PC_{71}BM$ are located rather on the side chains than on the aromatic part of the polymer. This is in contrast with the results obtained by E. Mena-Osteritz *et. al.*[35] In their D/A system, the preferential adsorption site for C_{60} is the aromatic part of the cyclothiophene. We thus believe that molecule-template interactions rely on specific couplings between D and A species.
In our case indeed, the profile of **Figure 3 (b)** shows that the apparent height of $PC_{71}BM$ randomly ranges from 0.4 to 0.6 nm above the PTB7 background. This shows that for $PC_{71}BM$, the adsorption geometry as well as the molecule-molecule or molecule-template electronic coupling, are not homogeneous, giving rise to some "energetic disorder" in the observed D/A junctions.

2.2 Charge transfer at the molecular scale in a D/A system under laser irradiation

2.2.1 Light-assisted scanning tunneling microscopy

We have developed a LA-STM setup (Light Assisted Scanning Tunneling Microscopy) which consists of a commercial STM (operating in ambient conditions) coupled through an optical fiber to a laser diode emitting at the wavelength $\lambda = 641$ nm. A focusing lens system reduces the diameter of the spot to about ten micrometers. In the constant current mode of the STM, we make use of the signal coming from the vertical retraction of the piezoelectric scanner during the irradiation of the tip, to center the laser spot at the tip-surface junction. The expected photocurrent I_φ is expressed by the following equation:[10]

$$I_\varphi = \sigma.|e|.Y.\Phi \qquad \text{where} \qquad Y = \frac{1/\tau_{_T}}{1/\tau_{_T} + 1/\tau_{_R}} \tag{1}$$

In equation 1, σ represents the absorption cross section of the molecule, Φ the flux of photons (per unit area and per unit of time) and Y the quantum yield. The latter depends on $1/\tau_{_T}$ and $1/\tau_{_R}$ (expressed as the number of electrons per unit of time), which correspond respectively to the tunnel transfer rate and the rate of relaxation of the excited state originating either from radiative, thermal or quenching effects. The estimation of the expected order of magnitude of the photocurrent for our D/A model system was made as follows: Under our illumination conditions (focused laser of *ca.* 50 mW of power), the flux of photons expressed by $\Phi = \mathcal{P}_{_S}/E_\varphi$ (with $\mathcal{P}_{_S}$, the laser power by surface unit and E_φ, the photon energy)

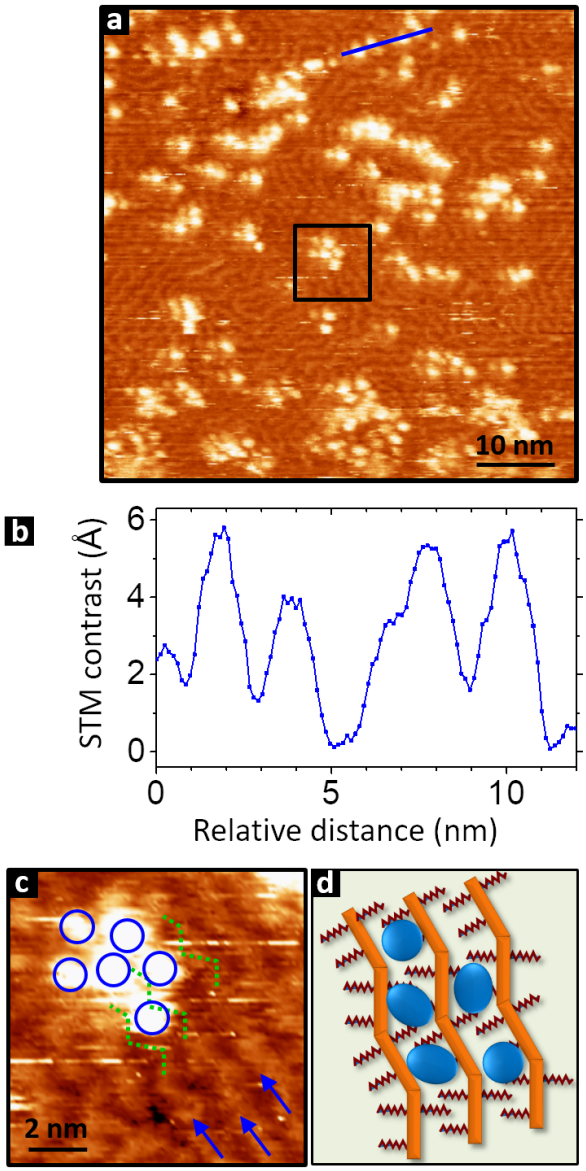

Figure 3: (a) STM image (60×60 nm^2; $V_t = +0.6$ V; $I_t = 50$ pA) showing the $PC_{71}BM$ islands resulting from drop casting on PTB7/Au(111). (b) Cross section extracted from image (a). (c) Magnified image of PTB7/$PC_{71}BM$ junctions highlighting the preferential adsorption sites of $PC_{71}BM$ on PTB7 (template effect). (d) Sketch of the D/A system.

equals 3×10^8 photons.nm^{-2}.s^{-1}. The absorption cross section of the donor (PTB7), estimated from its molar extinction coefficient (measured by UV-Vis absorption spectroscopy), is $\sigma = 0.5$ nm^2 at the excitation wavelength of the laser. We deduce N_φ, the number of photons absorbed per unit of time and per molecule: $N_\varphi = \Phi \times \sigma = 1.5 \times 10^8$ photons.s^{-1}. Experimentally, the characteristic relaxation time of the excited state τ_R ranges from 10 fs to 100 fs.[36] On the other hand, the quantum theory of the tunneling effect leads to values of τ_T comprised between 10 fs and 10 ps. The order of magnitude of the quantum yield can thus vary from 1 (in the ideal situation where each absorbed photon would be converted into an elementary electron of charge $|e|$ collected by the tip of the STM), to 10^{-3}. Then, the expected value of the photo-induced current I_φ could not exceed 10 pA and could be as low as 10 fA.
Extracting this signal (which is close to the noise level of the STM detection chain) by continuous irradiation of the surface is expected to be tricky, in addition to the heat dissipation issue that the STM junction would experience under permanent high power illumination. We therefore opted for a differential measurement with a laser source of optical power $\mathcal{P}_o$ that can be modulated analogically over time at the angular frequency ω. The signal is then demodulated with a digital lock-in amplifier and we record the absolute value of the differential tunnel current induced by light excitation: $I_\omega = |I_t^{ON} - I_t^{OFF}|$

where the superscripts *ON* and *OFF* refer to illumination and dark phases, respectively. The full device is sketched in **Figure 4**.

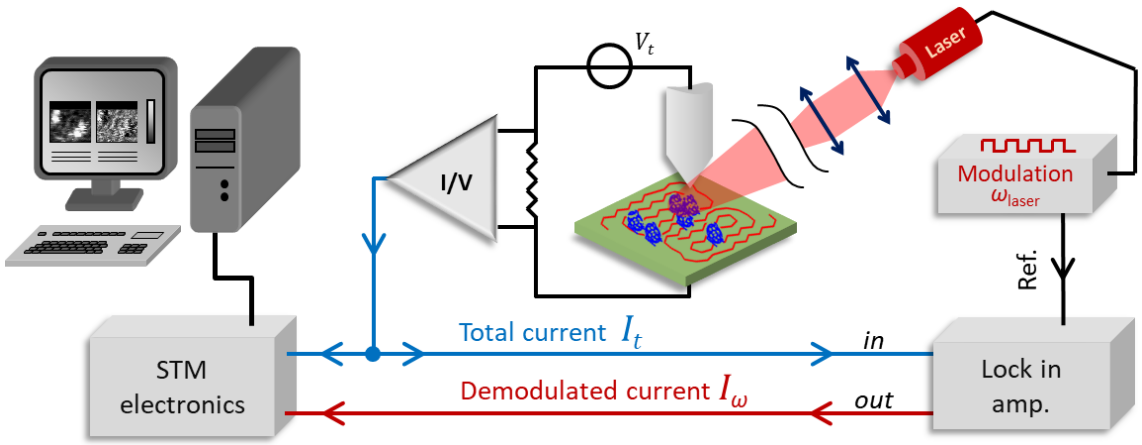

Figure 4: Scheme showing the principle of a light-assisted STM setup. The output of the STM's current/voltage (I/V) converter is sent into the lock-in amplifier which extracts the modulated component of the signal at the frequency of the laser irradiation.

The modulation frequency must be chosen outside the bandwidth of the feedback loop to prevent it from reacting to current variations related to the presence of the photo-induced component. Nevertheless, the working frequency must be set at the edge of the bandwidth of the I/V converter (measured around 10 kHz), so that the signal transmitted to the lock-in is not attenuated too much.
The modulation frequency of the laser is thus taken in the range 10 - 50 kHz. In this range, the detection limit of our LA-STM was measured at 7 fA. We are then able to record in parallel, the topographic signal and the mapping of the variations of the modulated current at the frequency of the laser. Since the characteristic times of the excitation phenomena are much faster than the laser illumination period (range 10 - 100 fs *versus* 1 - 100 μs respectively), we expect measuring the photo-electronic activity of our D/A system under stationary conditions of charge generation and transfer. However, as it will be described in the following, the modulated signal contains several contributions that should be separated, as far as possible, from each other.

2.3 Detection and analysis of photo-induced signals

LA-STM investigations carried out on the PTB7/$PC_{71}BM$ system, have been compared to the ones recorded on a SAM of adamantanethiol (AT) which does not absorb the light at the wavelength emitted by the laser. **Figure 5** shows the typical LA-STM results obtained on the two model systems. In both cases, the photocurrent variations superimpose well to the topographic signal of the molecules. In accordance with our expectations, the average photocurrent recorded for both systems is *ca.* 1 pA. However, getting such a high photo-induced signal with a non-photo-active system like AT raises questions about its origin. In the literature, the first results of STM under laser illumination have demonstrated the photothermal origin of this current.[37] The intermittent irradiation causes an alternation of dilations and contractions of the tip, which gives rise to fluctuations in the tunnel current following the modulation of the thickness of the tunnel barrier at the same frequency as that of the laser.[38] Such a photothermal current is proportional to the power of the laser as well as to the STM current setpoint, while it decreases as the modulation frequency of the laser increase.[39] It has also been shown that the polarization of light plays a role in the phenomenon.[40]
As the size of the laser spot is greatly larger than the thickness variations of the tunnel barrier upon intermittent irradiation, we can reasonably assume that the laser power is constant over the variations of the tip position. Then, the recorded modulated current I_ω can be expressed at the first order as:

$$I_\omega = |I_t(s - \Delta s) - I_t(s)| \approx \left| \frac{\partial I_t}{\partial s} \Delta s \right| \quad (2)$$

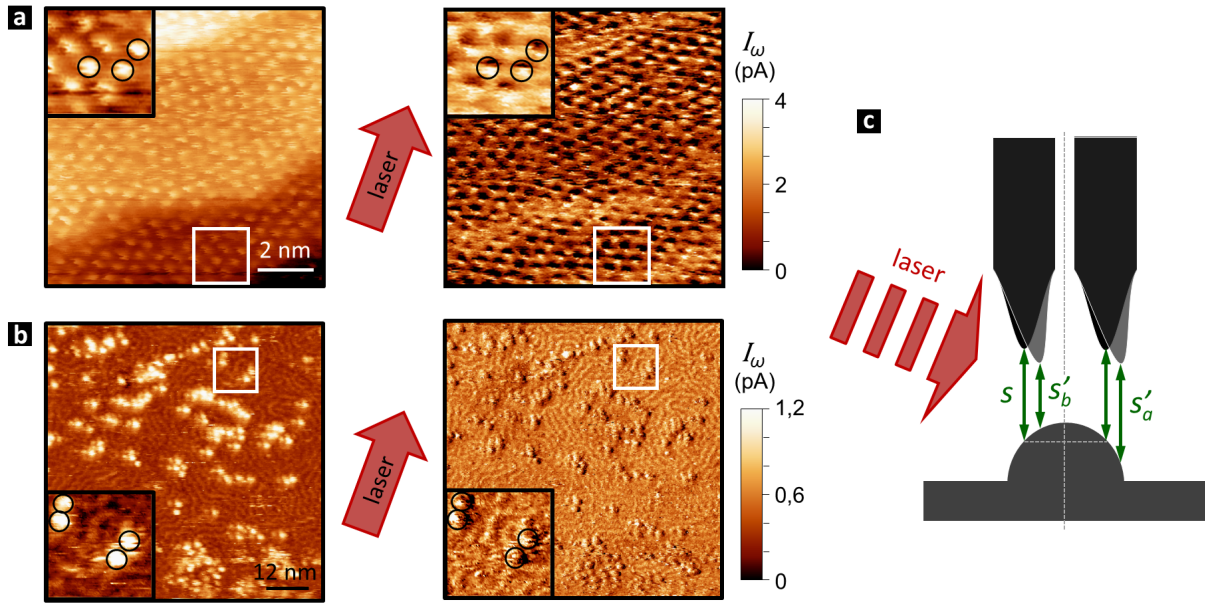

Figure 5: (a-b) Simultaneous LA-STM topographic images (left) and mapping of modulated photocurrent I_ω (right) provided by a lock-in amplifier set at the irradiation frequency f_L of the laser. (a) AT SAM on Au(111) (parameters: $\mathcal{P}_o = 75$ mW; $f_L = 12$ kHz; $V_t = 250$ mV; $I_t = 80$ pA). (b) D/A system based on PTB7/$PC_{71}BM$ on Au(111) (parameters: $\mathcal{P}_o = 75$ mW; $f_L = 20$ kHz; $V_t = 600$ mV; $I_t = 50$ pA). All the data have been recorded with *p*-polarized laser light. (c) Sketch illustrating the variation of the tunnel gap due to the photothermal effect.

where s is the thickness of the tunnel barrier in the dark; Δs is the maximum tip elongation due to the photothermal effect ($\Delta s > 0$). In the framework of the Tersoff and Hamann approximation,[41] assuming that the density of states (DOS) of the tip is constant, the tunnel current I_t can be expressed as:

$$I_t(s) = C \int_{E_F}^{E_F + e.V_t} \rho(E)\, e^{-\alpha.s}\, dE \tag{3}$$

where C is a positive constant, $\rho(E)$ is the sample's DOS, E_F is the Fermi level of the sample, V_t is the bias voltage of the sample relatively to the one of the tip, α is the decay factor relative to the electron tunneling transition probability. Combining Equation 2 and Equation 3, one obtain:

$$I_\omega = \alpha\, \Delta s\, I_t(s) \tag{4}$$

The contrast variations resulting from the photothermal phenomenon are thus proportional to the decay factor α which is itself proportional to the square root of the average tunnel barrier's height $\sqrt{\phi}$.[42] Then, in the case of the AT SAM, the contrast variations observed on the image of the photo-induced current can entirely be attributed to local variations of the tunnel barrier height.[43, 44, 45] In more detail, the modulated current maps I_ω obtained for both the AT SAM and the D/A system, show that the photocurrent contrast associated with each molecule forms adjacent bright and dark lobes. In addition, the orientation of these lobes faithfully follows the irradiation axis of the tunnel junction by the laser beam. We believe that this "shading effect" should result from a lateral oscillatory movement of the tip (sketched in **Figure 5 (c)**), its face exposed to the photon flux being subjected to greater expansion/contraction than its unexposed face. We point out that neither the tip length and shape nor the material it is made of (mechanically cut Pt:Ir tips *versus* electrochemically-etched gold tips) do significantly influence the shading effect. On the images, the effect is all the more visible that the tip presents a tapered apex. In this framework, The modulated current I^i_ω given by Equation 4 can then be rewritten as follows, for the two situations depicted in **Figure 5 (c)** for which the tip is located before ($i = b$) or after ($i = a$) a protrusion relatively to the laser beam axis:

$$I^i_\omega = \alpha\, (s'_i - s)\, I_t(s) \tag{5}$$

where s'_i represents the thickness of the tunnel barrier at maximum elongation for the tip positioned respectively before (s'_b) and after (s'_a) the protrusion. Obviously, $I^b_\omega > I^a_\omega$ since $s'_b < s'_a$, leading to expected contrast changes along the laser beam direction. We note that this effect depends on the shape of the protrusion. As a matter of comparison, **Figure S1** of the supporting information shows a photothermal LA-STM image recorded in the vicinity of a gold island covered with PTB7.
Unlike the photothermal process, charge transport in a photo-active D/A system should depend on the energetic configuration of HOMO and LUMO levels relative to the electrochemical potentials of the electrodes. The amplitude of the tunnel current resulting from molecular photo-excitation phenomena should therefore rely on the electrons flow direction, and consequently on the sign of the voltage applied to the junction (similarly to the photovoltaic effect). In order to highlight the photocurrent's component linked to molecular excitation phenomena, we have recorded the LA-STM images at two symmetrical potentials $+V_t$ and $-V_t$, by programming a double sweep of each scan line (**Figure 6**).

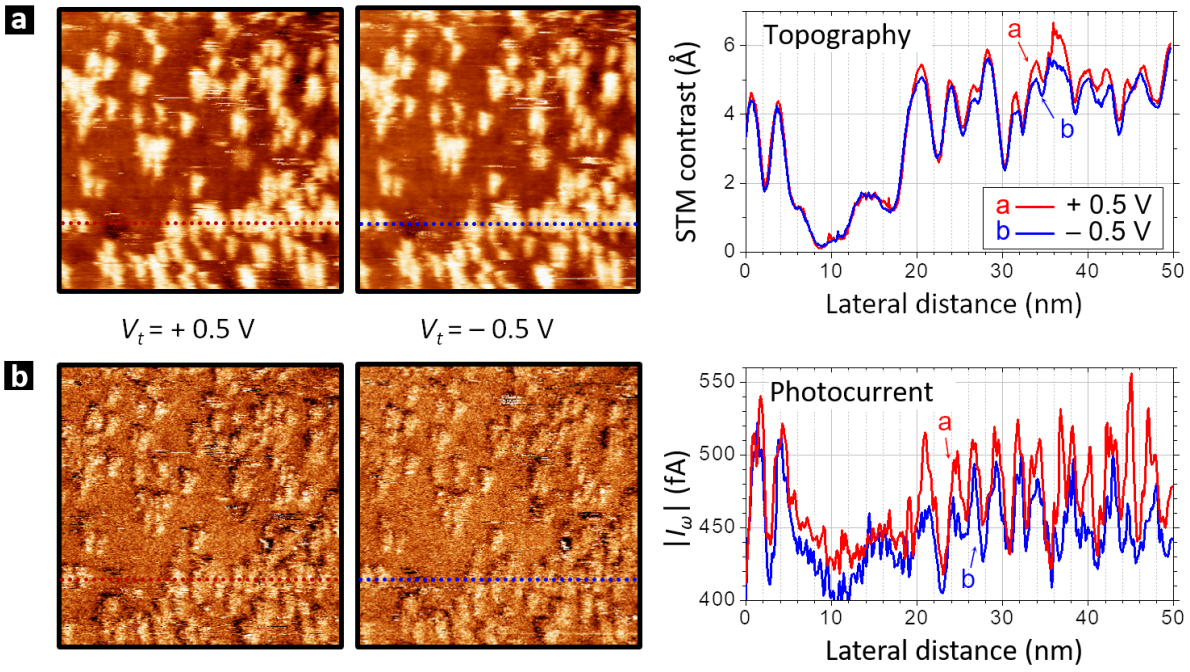

Figure 6: LA-STM images and profiles of the PTB7/$PC_{71}BM$ layer on Au(111) obtained by a double sweep of each scan line at $V_t = +0.5$ V and $V_t = -0.5$ V respectively. (a) Topography at $I_t = 10$ pA. (b) Modulated photocurrent map I_ω at $\mathcal{P}_o = 75$ mW and $f_L = 20$ kHz. The thermal drift of the STM under light irradiation is clearly visible, due to a relative long data acquisition time (*ca.* 20 mn per couple of images).

The profiles extracted from the I_ω maps show that the photo-induced current at +0.5 V is greater than the one measured at −0.5 V. The average disymmetry of the modulated current expressed as $\Delta I^\pm_\omega = |I^{+0.5V}_\omega| - |I^{-0.5V}_\omega|$ is *ca.* 40 fA at the $PC_{71}BM$ over PTB7 areas while this difference is three times lower on bare PTB7 zones. We assign this feature to the fingerprint of a photo-induced phenomenon superimposed on the photothermal signal detected at the D/A junctions. It should be noted that the amplitude of the disymmetry of $\Delta I^\pm_\omega$ measured on bare PTB7 is similar to that obtained on an AT SAM, as shown on **Figure S2** of the supporting information. This small signal shift probably corresponds to a combination of photo-induced phenomena of low dependence on V_t, and not related to molecular photoabsorption.[9] Moreover, the topographic profiles of **Figure 6 (a)** show, on the one hand, that the apparent height h_{STM} of $PC_{71}BM$ molecules, measured relatively to the PTB7 background, varies randomly and on the other hand, that the differential signal $\Delta h^\pm_{STM} = h^{+0.5V}_{STM} - h^{-0.5V}_{STM}$ is not null. The former observation shows that neither the adsorption geometry nor the electronic coupling between adsorbed molecules (or between molecule and host structure) are homogeneous, giving rise to a certain "energetic disorder" in the distribution of D/A junctions. This is in agreement with the observations made from KPFM measurements on D/A bulk heterojunctions, where local variations of SPV have been attributed

to local phase composition and/or morphology changes.[46] The latter observation could come from the fact that the shape and spatial extent of the molecular orbitals probed at +0.5 V (empty states) are not identical to those measured at −0.5 V (occupied states). Nevertheless, we observe no obvious correlation between the profiles $\Delta h^{\pm}_{STM}$ and $\Delta I^{\pm}_{\omega}$ (from **Figure 6 (b)**), which tends to prove that the disymmetry of the photocurrents measured at the D/A junction level, does not come from a variation between the exponential decays of the molecular states' wave functions probed in the tunnel junction at $+V_t$ and $-V_t$ respectively.
Subsequently, we have analyzed the spatial distribution of the differential photocurrent by superimposing on the topography, the image of $\Delta I^{\pm}_{\omega}$ generated by subtracting, pixel by pixel, the modulated-current maps obtained at +0,5 V and −0,5 V and applying a threshold corresponding to the sum of the measurement uncertainties (threshold estimated around 25 fA). The result is shown in **Figure 7**. One observe that the excess of photocurrent tends to localize at the borders of the $PC_{71}BM$ molecular domains as well as in the inter $PC_{71}BM$ spaces. Having discarded any correlation with the photothermal contrast, these more active areas in terms of photo-induced effects at the molecular level, are located at the interfaces between donor and acceptor moieties, which confirms that this photocurrent excess is correlated to photo-excitation events at the molecular scale.

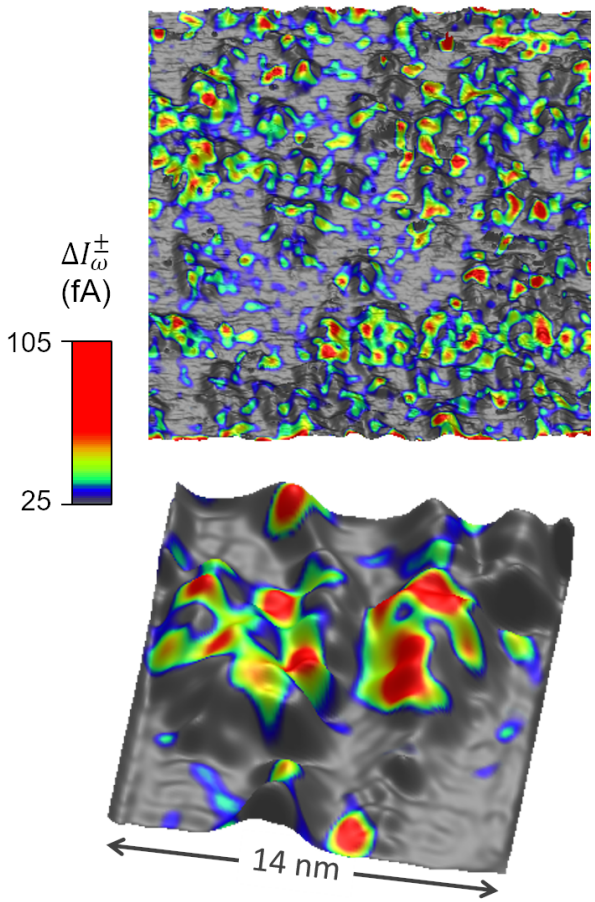

Figure 7: Top: Differential photocurrent map $\Delta I^{\pm}_{\omega}$ obtained above a threshold of 25 fA, superimposed to the STM topography of the PTB7/$PC_{71}BM$ system shown in Figure 6 (a). Bottom: Magnified image highlighting the distribution of the photocurrent in the vicinity of D/A junctions.

The origin of the photocurrent disymmetry with V_t lies in the electronic transport phenomenon through the molecular species located in the tunnel junction. In order to understand the mechanism, we have constructed the energy band diagram of the system (**Figure 8 (a)**). Taking into account that our experiments were driven in ambient conditions, we have considered a work function of 4.5 eV for gold. The energy levels of the molecules were taken from the recent literature.[47] We have then considered the model of metal/organic semiconductor interfaces in the framework of physisorbed organic systems.[48]

This model describes the energy positioning of the molecular orbitals with respect to the Fermi level of the metal, assuming that a charge transfer at the Au/PTB7 interface (which would lead to the filling of the polaronic levels of the polymer) would be energetically unfavored. This was also applied to physisorbed $PC_{71}BM$ over PTB7. We also assume that upon biasing of the junction, the entire voltage drop happens at the tunnel barrier. The absorption of a photon by the donor results in the creation of an electron/hole pair. The relaxation of these charges towards the available states of the surface (within a typical time scale of 10^1 to 10^2 fs) must be the predominant phenomenon facing the tunnel transfer towards the opposite electrode (within a typical time scale of 10^1 to 10^4 fs). This is consistent with the weak amplitude of the photo-excitation current that we have recorded. Nevertheless, the probability of exciton dissociation and electron transfer from the LUMO of PTB7 to the one of $PC_{71}BM$ is far from negligible. The residence time of this electron on the LUMO of $PC_{71}BM$ will be higher because of intrinsically weaker electronic couplings that the $PC_{71}BM$ holds with the two metallic electrodes.
At +0.5 V (**Figure 8 (b)**), the LUMO of the acceptor is very close to the resonance with the electrochemical potential of the tip. The presence of an electron on this level, in phase with the illumination periods of the tunnel junction, could energetically shift its position, leading to the disturbance of the resonant tunnel transport through this orbital (compared to the resonant transport situation in the dark phase, where this orbital is unoccupied). The modulation of the occupancy of the acceptor's LUMO level could thus explain the origin of such a modulated component of the photocurrent.
At −0.5 V (**Figure 8 (c)**), The tunnel transport is far from any resonance. The impact of photo-induced charge transfers between the LUMO states is therefore much lower than in the previous case, which could justify the disymmetry of I_ω with respect to the voltage sign inversion.

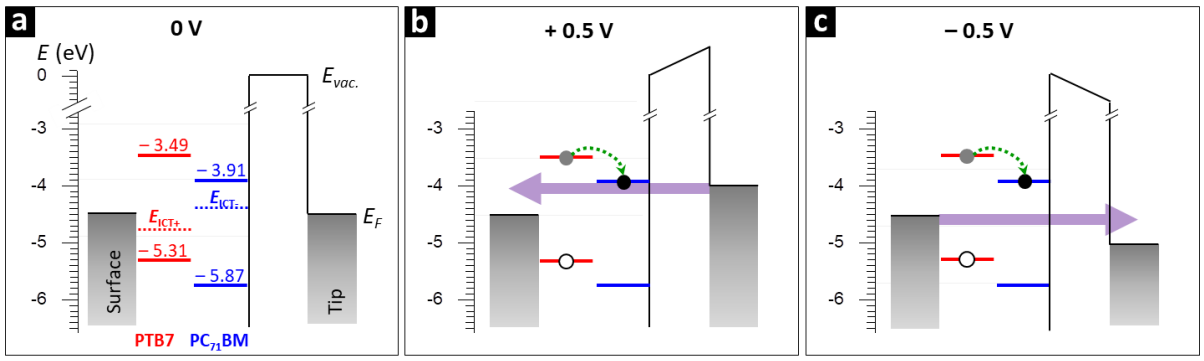

Figure 8: Energetic diagrams of the metal-PTB7-$PC_{71}BM$//metal junction. (a) Thermodynamic equilibrium situation. Charge transfer between gold and polaronic levels E_{ICT+} and E_{ICT-} of the polymer is found to be unfavored[48]. (b) Non-equilibrium situation under a bias voltage of $V_t = +0.5$ V. (c) Non-equilibrium situation under a bias voltage of $V_t = -0.5$ V.

In the **Section 3** of the supporting information, we propose a model based on the Tersoff and Hamann approximation showing that the $\Delta I_\omega^\pm$ maps still contain a combination of photothermal and photo-excitation effects. Moreover, according to our experimental observations, the model shows that the sign of $\Delta I_\omega^\pm$ is expected to be positive for LA-STM experiments carried out under high photothermal effects resulting from a high irradiation power source such as the one we have used. Nevertheless, it should be noted that the photothermal effects of LA-STM can be attenuated by using an interferometric system,[49] or by using an experimental configuration with two modulated lasers in phase opposition.[50]

3 Conclusion

Finally, by an all-solution approach, we have elaborated a donor/acceptor system made of a monolayer of PTB7 covered by a submonolayer of $PC_{71}BM$. Our STM data have shown the capability of the polymer to act as a template for the growth of $PC_{71}BM$ islands. We have developed a LA-STM setup capable of extracting photocurrents as low as 25 fA at the nanometric scale. Comparatively to the data obtained on a non photo-active system, we have demonstrated that the photo-induced current recorded on the D/A model system combine several contributions originating from photothermal effects (related to

both vertical and lateral expansion of the tip) and charge transfers between molecular species at their excited state. We have developed a procedure to enhance the molecular photo-excitation contribution and we have shown for the first time, a photocurrent mapping related to charge transfers between photo-excited species at the molecular level. All-in-all, the LA-STM experiments that we have carried out on the PTB7/$PC_{71}BM$ system converge towards the indirect detection of exciton dissociation at D/A interfaces, consistent with a perturbation of the tunnel transport through the partially unoccupied states of the molecules. This mechanism however needs to be experimentally consolidated through the determination of the energy levels involved in the system. STM measurements at other voltages should also provide more information about the intensity of the photo-induced perturbation. In perspective, comparative studies between different molecular systems, including the inverted system made of PTB7 covering a self-assembled monolayer of $PC_{71}BM$, could be considered in order to understand what are the most favorable conditions (at the molecular level) for charge separation and photocurrent generation.

4 Experimental Section

Surface treatments:
We used commercial substrates made of a 200 nm thick gold layer sputtered on mica sheets (purchased from Phasis, Geneva, Switzerland). They were cleaned by immersion in a ultrapure water/ethanol mixture (1/1; v/v) for 2 min and blown dry under an argon flow. The samples were flame annealed with a hydrogen torch. After this process, the surface exhibits large (111) oriented atomic terraces (typical width 100 nm). The annealing process is always achieved immediately before immersion of the substrates in the solution containing the molecules.

Chemicals:
PTB7 (Poly({4,8-bis[(2-ethylhexyl)oxy]benzo[1,2-b :4,5-b']dithiophene-2,6-diyl}{3-fluoro- 2-[(2-ethylhexyl)carbon
b]thiophenediyl}, powder, average molecular weight: 18000 kDa, Pd 1,75) and $PC_{71}BM$ (3'H-Cyclopropa[8,25][5,
C70-D5h(6)-3'butanoic acid, powder, purity $\geq$ 99.9%) were purchased from Ossila and used without further purification. Both molecules were dissolved in CB (chlorobenzene, anhydrous, purity $\geq$ 99.8%) purchased from Sigma-Aldrich and used as received. To avoid any contamination, glass vessels were cleaned by annealing in a hydrogen flame. PTB7 has ben dissolved in CB at an equivalent monomeric concentration of 1×10^{-4} mol.L^{-1}. The solution has been stirred at 40°C to ensure an optimized dispersion of the polymer chains in the solution. $PC_{71}BM$ has been dissolved in CB at a concentration of 1.5×10^{-4} mol.L^{-1}. Both solutions were used less than one hour after preparation in order to avoid degradation or aggregation.

Molecular self-assembly processes:
Single layers of PTB7 and $PC_{71}BM$ on Au(111) have been obtained by drop casting as follows: first, the gold substrates are annealed at 80°C. Then, a droplet of solution (0.6 μL per mm^2) is deposited on the surface. The drying time is typically of a few tens of seconds. By this method, the surface is mainly covered by single layers of molecules in a reproducible way. Thicker layers are found only in highly concentrated areas, *i.e.* where the droplet has lastly dried. PTB7/$PC_{71}BM$ systems were made through a sequential drop coating process. The deposition of the polymer layer is followed by the $PC_{71}BM$ one, using the aforementioned conditions. The gradient of concentration that occurs upon drying tunes the molecular density on the surface.

STM analysis:
STM studies were performed under ambient conditions using a Molecular Imaging PicoScan microscope. STM image acquisition was done in the constant current mode with the following typical parameters: current set point I_t ranging from 10 pA to 100 pA; bias voltage V_t ranging from 100 mV to 800 mV. Image processing was carried out with the free WSxM software (Nanotec Electrónica).[51] Unless explained otherwise, tips were cut from 0.25 mm wide Pt:Ir (80:20) wires.

Supporting Information

Supporting Information is available from the Wiley Online Library or from the author.

Acknowledgements
ANR (Agence Nationale de la Recherche) and CGI (Commissariat à l'Investissement d'Avenir) are gratefully acknowledged for their financial support of this work through Labex SEAM (Science and Engineering for Advanced Materials and devices) ANR 11 LABX 086, ANR 11 IDEX 05 02. Special thanks are addressed to Fabrice Charra (CEA Saclay) for fruitful discussions around the LA-STM experimental setup and results.

References

[1] S. Wieghold, J. Li, P. Simon, M. Krause, Y. Avlasevich, C. Li, J. A. Garrido, U. Heiz, P. Samorì, K. Müllen, F. Esch, J. V. Barth, C.-A. Palma, *Nature Commun.* **2016**, *7* 10700.

[2] D. A. Bonnell, D. Basov, M. Bode, U. Diebold, S. V. Kalinin, V. Madhavan, L. Novotny, M. Salmeron, U. D. Schwarz, P. S. Weiss, *Rev. Modern Phys.* **2012**, *84* 1343.

[3] H. Imada, K. Miwa, M. Imai-Imada, S. Kawahara, K. Kimura, Y. Kim, *Nature* **2016**, *538* 364.

[4] Z. C. Dong, X. L. Zhang, H. Y. Gao, Y. Luo, C. Zhang, L. G. Chen, R. Zhang, X. Tao, Y. Zhang, Y. J. L., J. G. Hou, *Nat. Photonics* **2010**, *4* 50.

[5] E. Escasaín, E. López-Elvira, A. M. Baró, J. Colchero, E. Palacios-Lidón, *J. Phys. Chem. C* **2012**, *116* 17919.

[6] P. A. Cox, M. S. Glaz, J. S. Harrison, S. R. Peurifoy, D. C. Coffey, D. S. Ginger, *J. Phys. Chem. Lett.* **2015**, *6* 2852.

[7] F. Fuchs, F. Caffy, R. Demadrille, T. Mélin, B. Grévin, *ACS Nano* **2016**, *10* 739.

[8] A. Liscio, V. Palermo, P. Samorì, *Acc. Chem. Res.* **2010**, *43* 541.

[9] S. Grafström, *J. Appl Phys.* **2002**, *91* 1717.

[10] O. Probst, S. Dey, J. Fritz, S. Grafström, T. Hagen, J. Kowalski, G. Zu Putlitz, R. Neumann, *Laser-Assisted Scanning Tunneling Microscopy Studies of Thin Ordered Molecular Layers*, 269–274, Springer Netherlands, ISBN 978-94-011-0423-4, **1995**.

[11] D. Smith, R. Owens, *Appl. Phys. Lett.* **2000**, *76* 3825.

[12] I. V. Pechenezhskiy, X. Hong, G. D. Nguyen, J. E. Dahl, R. M. Carlson, F. Wang, M. F. Crommie, *Phys. Rev. Lett.* **2013**, *111* 126101.

[13] S. Grafström, P. Schuller, J. Kowalski, R. Neumann, *Appl. Phys. A* **1998**, *66* 1237.

[14] D. Fichou, F. Charra, A. O. Gusev, *Adv. Mater.* **2001**, *13* 555.

[15] S. Wu, N. Ogawa, W. Ho, *Science* **2006**, *312* 1362.

[16] J. B. Ballard, E. S. Carmichael, D. Shi, J. W. Lyding, M. Gruebele, *Nano lett.* **2006**, *6* 45.

[17] L. Nienhaus, J. J. Goings, D. Nguyen, S. Wieghold, J. W. Lyding, X. Li, M. Gruebele, *J. Am. Chem. Soc.* **2015**, *137* 14743.

[18] S. Park, J. Jeong, G. Hyun, M. Kim, H. Lee, Y. Yi, *Sci. Rep.* **2016**, *6* 35262.

[19] R. Otero, D. Écija, G. Fernández, J. M. Gallego, L. Sánchez, N. Martín, R. Miranda, *Nano Lett.* **2007**, *7*, 9 2602.

[20] J. M. Szarko, B. S. Rolczynski, S. J. Lou, T. Xu, J. Strzalka, T. J. Marks, L. Yu, L. X. Chen, *Adv. Funct. Mater.* **2014**, *24* 10.

[21] C. Musumeci, R. Borgani, J. Bergqvist, O. Inganäs, D. Haviland, *RSC Adv.* **2017**, *7* 46313.

[22] A. Muraoka, M. Fujii, K. Mishima, H. Matsunaga, H. Benten, H. Ohkita, S. Ito, K. Yamashita, *Phys. Chem. Chem. Phys.* **2018**, *20* 12193.

[23] T. Ferron, M. Waldrip, M. Pope, B. A. Collins, *J. Mater. Chem. A* **2019**, *7* 4536.

[24] I. Caballero-Quintana, J.-L. Maldonado, M.-A. Meneses-Nava, O. Barbosa-García, J. Valenzuela-Benavides, A. Bousseksou, *Adv. Electron. Mater.* **2019**, *5* 1800499.

[25] S. M. Ryno, C. Risko, *Phys. Chem. Chem. Phys.* **2019**, *21* 7802.

[26] E. Mena-Osteritz, A. Meyer, B. M. W. Langeveld-Voss, R. A. J. Janssen, E. W. Meijer, P. Bäuerle, *Angew. Chem. Int. Ed.* **2000**, *39*, 15 2679.

[27] P. Renaud, B. Mickael, R. Patrice, B. Robert, G. Benjamin, *Synth. Met.* **2004**, *146*, 3 311, organic Field-Effect Transistors: Towards Molecular Scale. Proceedings of Symposium E. E-MRS Spring Meeting.

[28] W. Chen, T. Xu, F. He, W. Wang, C. Wang, J. Strzalka, Y. Liu, J. Wen, D. J. Miller, J. Chen, K. Hong, L. Yu, S. B. Darling, *Nano Lett.* **2011**, *11*, 9 3707, pMID: 21823620.

[29] M. Williams, N. R. Tummala, S. G. Aziz, C. Risko, J.-L. Brédas, *J. Phys. Chem. Lett.* **2014**, *5*, 19 3427.

[30] L. Sánchez, R. Otero, J. M. Gallego, R. Miranda, N. Martín, *Chem. Rev.* **2009**, *109*, 5 2081, pMID: 19253947.

[31] D. Écija, R. Otero, L. Sánchez, J. Gallego, Y. Wang, M. Alcamí, F. Martín, N. Martín, R. Miranda, *Angew. Chem. Int. Ed.* **2007**, *46*, 41 7874.

[32] W.-J. Li, Y.-Y. Du, H.-J. Zhang, G.-H. Chen, C.-Q. Sheng, R. Wu, J.-O. Wang, H.-J. Qian, K. Ibrahim, P.-M. He, H.-N. Li, *Surf. Sci.* **2016**, *654* 8.

[33] L. Tskipuri, Q. Shao, J. Reutt-Robey, *J. Phys. Chem. C* **2012**, *116*, 41 21874.

[34] H. Cao, M.-P. Van Den Eede, G. Koeckelberghs, K. S. Mali, S. De Feyter, *Chem. Commun.* **2017**, *53* 153.

[35] E. Mena-Osteritz, P. Bäuerle, *Adv. Mater.* **2006**, *18*, 4 447.

[36] P. Avouris, B. N. Persson, *J. Phys. Chem.* **1984**, *88* 837.

[37] N. M. Amer, A. Skumanich, D. Ripple, *Appl. Phys. Lett.* **1986**, *49* 137.

[38] S. Grafström, P. Schuller, J. Kowalski, R. Neumann, *J. Appl. Phys.* **1998**, *83* 3453.

[39] S. M. Landi, A. V. Bragas, J. A. Coy, O. E. Martínez, *Ultramicroscopy* **1999**, *77* 207.

[40] A. Bragas, S. Landi, J. Coy, O. Martìnez, *J. Appl. Phys.* **1997**, *82* 4153.

[41] J. Tersoff, D. R. Hamann, *Phys. Rev. B* **1985**, *31* 805.

[42] C. J. Chen, *Introduction to Scanning Tunneling Microscopy*, Monographs on the Physics and Chemistry of Materials. Oxford University Press, 2 edition, **2007**.

[43] O. Probst, S. Grafström, J. Fritz, S. Dey, J. Kowalski, R. Neumann, M. Wörtge, G. Zu Putlitz, *Appl. Phys. A* **1994**, *59* 109.

[44] P. Han, A. R. Kurland, A. N. Giordano, S. U. Nanayakkara, M. M. Blake, C. M. Pochas, P. S. Weiss, *ACS Nano* **2009**, *3* 3115.

[45] J. C. Thomas, D. P. Goronzy, K. Dragomiretskiy, D. Zosso, J. Gilles, S. J. Osher, A. L. Bertozzi, P. S. Weiss, *ACS Nano* **2016**, *10* 5446.

[46] B. Grévin, O. Bardagot, R. Demadrille, *Beilstein J. Nanotechnol.* **2020**, *11* 323.

[47] R. Sharma, H. Lee, V. Gupta, H. Kim, M. Kumar, C. Sharma, S. Chand, S. Yoo, D. Gupta, *Org. Electron.* **2016**, *34* 111.

[48] S. Braun, W. R. Salaneck, M. Fahlman, *Adv. Mater.* **2009**, *21* 1450.

[49] S. M. Landi, O. E. Martínez, *J. Appl. Phys.* **2000**, *88* 4840.

[50] S. Grafström, J. Kowalski, R. Neumann, O. Probst, M. Wörtge, *J. Vac. Sci. Technol. B* **1991**, *9* 568.

[51] I. Horcas, R. Fernández, J. M. Gómez-Rodríguez, J. Colchero, J. Gómez-Herrero, A. M. Baro, *Rev. Sci. Instrum.* **2007**, *78* 013705.

Table of Contents

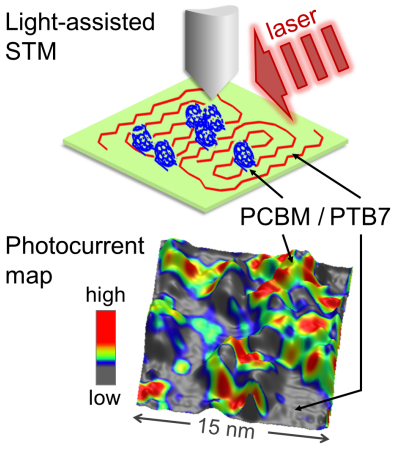

A 2D assembly of PTB7 (donor) and $PC_{71}BM$ (acceptor) has been elaborated by templated growth in solution. Scanning tunneling microscopy under light irradiation has permitted to record photocurrent maps of the donor/acceptor system with a nanometric resolution. Photocurrent peaks detected at the donor/acceptor interfaces give evidence for charge transfers between molecular species at their excited state.